Evaluating planetary boundary-layer schemes and large-eddy simulations with measurements from a 250-m meteorological mast

Peña, Alfredo; Hahmann, Andrea N.

Published in:
Journal of Physics: Conference Series

Link to article, DOI:
10.1088/1742-6596/1618/6/062001

Publication date:
2020

Document Version
Publisher's PDF, also known as Version of record

Journal of Physics: Conference Series

Evaluating planetary boundary-layer schemes and large-eddy simulations with measurements from a 250-m meteorological mast

Evaluating planetary boundary-layer schemes and large-eddy simulations with measurements from a 250-m meteorological mast

Alfredo Peña and Andrea N. Hahmann
DTU Wind Energy, Technical University of Denmark, Risø campus, Roskilde, Denmark
E-mail: aldi@dtu.dk

Abstract. We evaluate the performance of six planetary boundary layer (PBL) schemes and a large-eddy simulation (LES) for the characterization of the neutral PBL through idealized simulations using the Weather Research and Forecasting model. The evaluation is performed by comparison with sonic anemometer measurements from a 250-m tall meteorological tower that observes close-to-homogeneous winds under the predominant westerlies. All simulations show similar behavior for the vertical temperature profile except for one that uses a non-local PBL scheme, which is known to produce excessive vertical mixing. Within the range of measurements of the tower and except for a PBL scheme that produces a too low jet, the simulations using PBL schemes, which were developed to simulate the nighttime atmosphere, generally show the largest deviations from the observed wind speeds. As expected within the surface layer, the LES shows excessive vertical shear. More importantly, we find that two PBL schemes that use their own surface-layer scheme are effectively reducing the surface roughness. When looking at the vertical profile of momentum exchange coefficient, we find very good agreement between a local and a non-local PBL scheme within the bulk of the PBL, the highest values for the simulation with the PBL scheme showing excessive vertical mixing and the lowest values for that most suitable for nighttime conditions. The comparison with the observed turbulent kinetic energy reveals a good match between the LES and a simulation using a local PBL scheme and a general underestimation (overestimation) of turbulence within the range of measurements by the PBL schemes (LES).

1. Introduction

Planetary boundary layer (PBL) schemes are used in numerical weather prediction (NWP) models to simulate mesoscale processes as accurately as possible, because it is still not computationally affordable to predict weather with higher fidelity models, such as those that have the ability to perform large-eddy simulations (LESs). Turbulent eddies are responsible for the exchanges of moisture, heat, and momentum occurring within the PBL. However, they operate on spatio-temporal scales that cannot be explicitly represented using the grid resolution and time steps of most NWP models [1]. Therefore, we want to represent the effect of the eddies on the turbulent processes within the PBL using PBL schemes.

The effect on the wind speed of simulations using different PBL schemes has been intercompared and evaluated against observations of atmospheric parameters in many different studies [2, 3]. In the majority of these studies, it is difficult to adequately evaluate the ability of the PBL scheme to characterize the PBL processes because the PBL schemes have been

integrated into a real-time atmospheric modeling system and thus depend on many other factors. For example, the quality of the boundary and lateral conditions from reanalysis datasets, and the ability of the modeler to isolate the effects of the PBL schemes from those of the model chain. The PBL schemes have also been evaluated against the results from LES in the past [4]. However, the PBL schemes compared in those are not the same as those used in current modeling systems and no observations were simultaneously used for comparison.

Evaluating the performance of PBL schemes is of high importance for wind energy. Most long-term time series of wind characteristics used for wind resource assessment are derived from NWP models that can be run using many PBL schemes and other physical parameterizations. A recent example of such usage is the New European Wind Atlas project in which a numerical wind atlas was created based on the outputs of the Weather Research and Forecasting (WRF) model [5]. The PBL scheme was selected after sensitivity studies were carried out with a number of PBL schemes as well as other physics and configuration options of the model [6]. Different PBL schemes in these wind atlas simulations can change the long-term mean wind speed by as much as 1 m s^{-1} depending on surface roughness length [6]. Recent articles [6, 7] have shown that a particular PBL scheme [8] has the best skill for long-term wind speed simulation, but in many cases this is related to the internal representation of surface roughness length in the surface-layer scheme. Many simulations for sites in Northern Europe were also compared [9], but found no direct relationship between PBL scheme and various wind speed verification statistics. In this last study, the use of different models, grid spacing, land use maps, etc. confounds the results.

Here, we evaluate the ability of a number of PBL schemes that are integrated into a commonly used atmospheric modeling system to characterize the neutral PBL by performing idealized simulations (over flat and homogeneous surface conditions) and we also perform a large-eddy simulation of the same neutral idealized PBL. Results of both types of simulations are further compared to high-quality observations of the atmospheric flow, available from instruments deployed on a 250-m meteorological mast located at the National Test Site for Large Wind Turbines in Østerild, northern Denmark. Measurements from the mast show, for the predominant and nearly homogeneous flow conditions, an abundance of neutral stability conditions and statistics with regards to means and turbulence parameters were already computed [10], which are here used as benchmark for the simulations.

2. Methodology

We run all the idealized simulations of the neutral PBL using the Weather Research and Forecasting (WRF) model version 4.1.2. For the simulations based on PBL schemes, we use a domain with dimensions $(L_x, L_y, L_z) = (100, 100, 2)$ km, x and y being the horizontal directions and z the vertical direction. For the LES (also known as WRF-LES), we use $(L_x, L_y, L_z) = (10, 10, 2)$ km. The horizontal resolution in both directions, Δx and Δy, used for the simulations based on PBL schemes is set to 1 km to mimic the resolutions used for mesoscale modeling with such schemes. For the LES, we use $\Delta x = \Delta y = 100$ m similarly to a previous WRF study [11]. For both LES and PBL simulations, we use the same vertical levels; vertical grid spacing of ≈5 m is kept constant up to about 250 m, which is the range covering the meteorological mast measurements, then it is stretched out up to ≈900 m, where it reaches ≈35 m, and kept constant upwards. Figure 1-left shows the vertical resolution as a function of the vertical level, where the three regions described above can be seen.

For both LES and PBL simulations, the domain bottom is flat and we assign the surface roughness length z_0 equal to the value estimated from the Østerild observations under close-to-neutral surface atmospheric conditions within the close-to-homogeneous sector, i.e., $z_0 = 0.2492$ m (see Sect. 3 for details). The Coriolis parameter is set to the value corresponding to the latitude of the Østerild meteorological mast location (57.0489°). The time step used for the

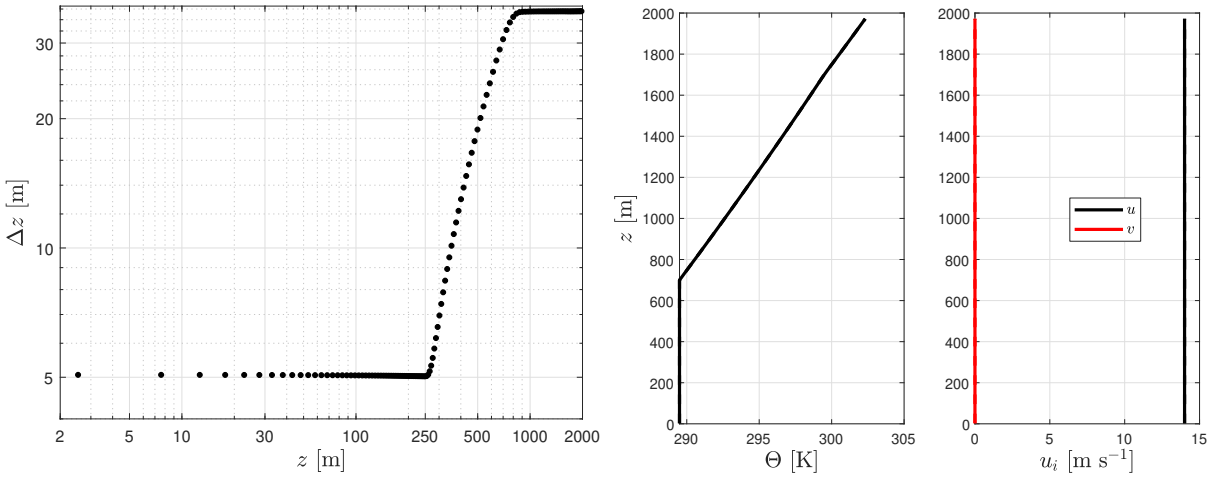

Figure 1. (Left frame) Grid spacing in the vertical direction as function of the vertical level. (Right frames) The initial vertical profiles of potential temperature and horizontal velocity components used in all the simulations

LES is 1 s and for the simulations based on PBL schemes, this is increased to 6 s. LES is performed using the subgrid-scale (SGS) model of Deardoff [12] with the prognostic equation for the subgrid turbulent kinetic energy (TKE).

The simulations are setup similarly to a previous intercomparison study on LESs [13]. All simulations are initialized assuming a dry atmosphere. The initial temperature is kept constant (289.5 K) up to 700 m and then an inversion of 10 K km^{-1} is imposed. Also for all simulations, the initial u_x- and u_y-velocity components, aligned with the x- and y-axis, respectively, are kept constant throughout the PBL, with values of 14 and 0 m s^{-1}, respectively (see Fig. 1-right frames). The 14 m s^{-1} value is subjectively chosen because it is just higher than the ensemble-average wind speed observed at the 241-m sonic anemometer during the close-to-neutral and homogeneous conditions at Østerild.

As shown in Table 1, we perform a LES and six other simulations corresponding to six commonly used PBL schemes. Three of the PBL schemes use the local mixing approach and the other three are non-local. The table also summarizes some other features of the PBL schemes, e.g., those with regards to the momentum diffusivity coefficient K_m formulation. For the non-local PBL schemes, K_m is constrained within the PBL,

$$K_m = \kappa v_s z \left(1 - \frac{z}{h}\right)^2, \tag{1}$$

where h is the PBL height, v_s a velocity scale, and κ the von Kármán constant (0.4). For both the Medium-Range Forecast (MRF) and Yonsei University (YSU) schemes, $v_s = w_s$, where w_s is the mixed-layer velocity scale; in MRF, this is defined as $w_s = u_* \phi_m^{-1}$, being u_* and ϕ_m the friction velocity and dimensionless wind shear, respectively, whereas in YSU, $w_s = \left(u_*^3 + \phi_m \kappa w_{*b}^3 z/h\right)^{1/3}$, being w_{*b} the convective velocity scale of most air. Notice that for the neutral and dry PBL, $w_{*b} = 0$ m s^{-1} and $\phi_m = 1$ and so w_s is the same in MRF and YSU. The main difference between MRF and YSU is however the addition of an asymptotic entrainment flux term at the inversion layer in the latter scheme. The Asymmetrical Convective Model version 2 (ACM2) combines a non-local approach, which represents large-scale transport, and a local eddy diffusivity approach, which represents the subgrid-scale components. In the neutral PBL, K_m in ACM2 is equal to that in MRF because a stability-dependent correction used in ACM2 is equal to one.

The Mellor-Yamada-Jankic (MYJ) and the Mellor-Yamada-Nakanishi-Niino version 2 (MYNN2) schemes are both local and based on the original approximations by Mellor-Yamada (MY) of turbulent processes within the PBL [14]. Particularly, the so-called level 2 approximation in MY expresses the momentum exchange as

$$K_m = leS_m, \tag{2}$$

where l is a master length scale, e^2 is twice the turbulent kinetic energy k, and S_m a stability function for momentum. One of the main differences between MYJ and MYNN2 with respect to MY is related to the expressions for l. In MY, l is diagnosed as a combination of a surface-layer and a turbulent- and h-dependent length scale. MYNN2 uses a similar concept but introduces, i.a., atmospheric stability corrections into the surface-layer length scale and a third length scale related to the buoyancy length scale, which is only effective in stable conditions. In MYJ, l follows the idea of MY, except that the turbulent length scale is limited to 80 m. Another fashion of a local approximation is that used by the quasi-normal scale elimination (QNSE) scheme, which is a spectral model in the k–ϵ-like format. The momentum diffusivity is expressed as

$$K_m = \alpha_m C_\mu \frac{k^2}{\epsilon}, \tag{3}$$

where α_m is a normalized eddy viscosity, C_μ a constant, and ϵ the rate of dissipation of k.

PBL scheme	surface layer	simulation name	some details and main reference
LES (no PBL)	MOST1	LES-MOST1	
MRF	MOST1	MRF-MOST1	non-local, $K_m(h, z, w_s)$ [15]
YSU	MOST1	YSU-MOST1	similar to MRF with entrainment flux at h [16]
ACM2	MOST1	ACM-MOST1	hybrid: upward and downward vertical transport + $K_m(h, z, \phi_m, u_*)$ [17]
MYJ	MYJ	MYJ-MYJ	local, prognosed e, $K_m(l, e, S_m)$ [18]
MYNN2	MOST1	MYNN2-MOST1	local, prognosed e, $K_m(l, e, S_m)$ [8]
QNSE	QNSE	QNSE-QNSE	local, an improved k–ϵ [19]

Table 1. A description of the PBL and surface-layer schemes used for the set of idealized simulations in WRF. Further details are given in the text

For the LES, Monin-Obukhov similarity theory (MOST) [20] is applied at the surface through an in-built WRF surface-layer scheme that is based on the scheme used by the MM5 model (hereafter MOST1). We also use two other surface-layer schemes; this is because some PBL schemes can only be used in the WRF model with their own surface-layer schemes, e.g., MYJ and QNSE, and others can be used with several surface-layer schemes, e.g., MYNN2. All simulations are performed for 24 h and a constant heat flux of 0 K m s^{-1} is always imposed at the surface.

All simulations are performed using periodic boundary conditions, which helps triggering turbulence in the LES and the PBL runs to develop the boundary layer. For all simulations instantaneous values of all relevant variables are output every 1 h for the whole domain. All parameters analyzed correspond to spatial averages over the whole domain at a given time.

3. The Østerild measurements

The measurements from the south lightning mast at Østerild, located in northern Jutland, Denmark have been described in detail ([10]). Here, we use 10-min statistics of the measurements

from the Metek USA-1 sonic anemometers at 7, 37, 103, 175, and 231 m. We filter the data to use only periods of westerlies, which are the most predominant at the site, specifically for wind directions within 270±15° based on the 37-m level. Within this direction range, there is a forest clearance and we can assume that the flow can be considered to be close-to-homogeneous. The behavior of the vertical wind profile and the dimensionless wind shear follow well the MOST predictions for the first tens of meters [10], which makes our assumption reasonable. Note that although the flow can be assumed horizontally homogeneous close to the surface, mesoscale gradients dominate over turbulence at higher levels. Further we select only 10-min statistics correspondent to close-to-neutral conditions based on the 37-m measurements, i.e., $|37\ \mathrm{m}/L| \leq 0.05$, where L is the Obukhov length and mean wind speeds above 3 m s^{-1}. The selection results in 3686 10-min periods. The surface roughness is estimated for each of those 10-min periods using the 37-m measurements as

$$z_0 = \frac{37\ \mathrm{m}}{\exp\left(\kappa U/u_*\right)}, \tag{4}$$

where U is the horizontal wind speed. The average surface roughness (0.2492 m) is found as $\exp\left(\overline{\ln(z_0)}\right)$, where the overline represents a mean. We estimate the momentum exchange from the sonic-anemometer measurements using the mixing-length concept as:

$$K_m = u_*^2 \left(\frac{dU}{dz}\right)^{-1}. \tag{5}$$

In order to compute K_m at all sonic anemometer levels, we compute dU/dz by fitting a polynomial form to the wind speed measurements [21].

4. Results

For the LES, we select the outputs at 11 h because, at this hour, we find the highest value of spatial-averaged horizontal wind speed, $\langle U\rangle = \left(\langle u_x\rangle^2 + \langle u_y\rangle^2\right)^{1/2}$, where $\langle\rangle$ represents a spatial average, within the 24-h simulation period. For simulations using PBL schemes, the horizontal wind speed maximum is always found either at hour 10 or 11. Therefore, we choose to extract the outputs for all simulations with PBL schemes at 10 h. The simulation time is long enough to capture the inertial oscillations that are characteristic under neutral atmospheric conditions [13].

Figure 2 illustrates spatial-average vertical profiles of the potential temperature (left frame) and the horizontal wind speed (right frame) for the set of simulations. When looking at the whole PBL, we find very good agreement for the potential temperature between all simulations, with MRF-MOST1 being the most different among them. MRF was found to show excessive vertical mixing that lead to a too deep PBL height, particularly under strong wind conditions [22]. Although the relative differences in wind speed are not that large between the simulations, YSU-MOST1 peaks the lowest and seems to be the one that differs the most with the observations. In the mechanically induced forced convection regime, YSU was found to decrease boundary-layer mixing [16]. MRF-MOST1 peaks the highest, as expected from the location of the temperature inversion and the problems above mentioned. MYJ-MYJ follows very closely the LES in the middle part of the PBL, and QNSE-QNSE and particularly ACM-MOST1, MRF-MOST1, and MYNN2-MOST1 seem to match the observations the closest. Table 2 provides a quantitative assessment of the performance of the simulations by computing both the mean absolute error and the root mean square error between the wind speed observations and the model results, interpolated at the observational levels, across the five measured heights.

When looking at the normalized wind speed U/u_* (Fig. 3-left frame), we found that LES-MOST1 and particularly YSU-MOST1 show excessive vertical wind shear in the first 250 m when

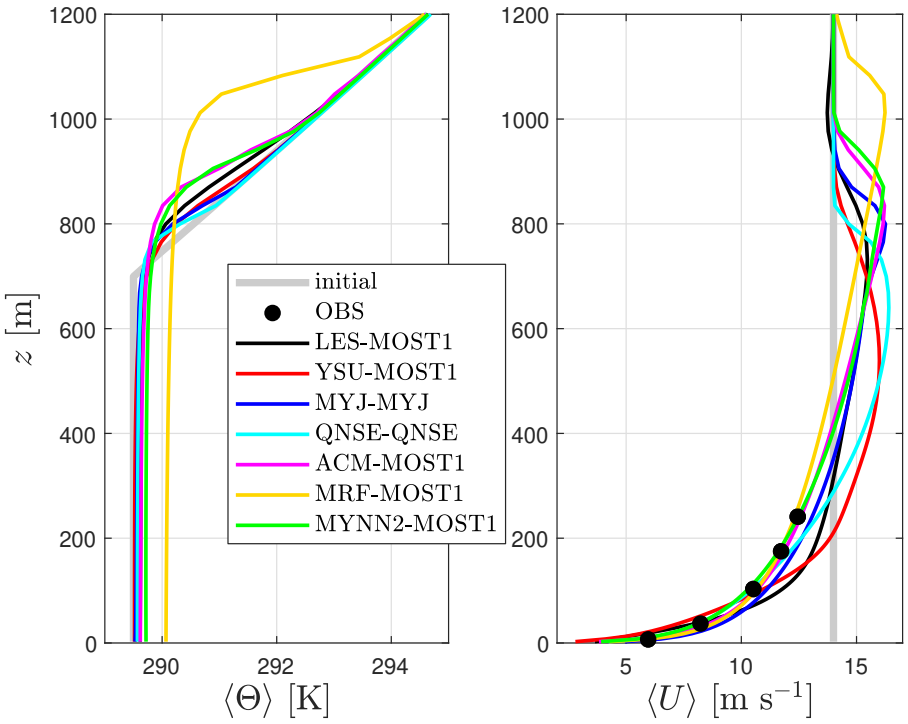

Figure 2. Spatial-average vertical profiles of potential temperature (left frame) and wind speed (right frame) within the PBL. Observations (OBS) are represented by the black markers and simulations by the colored lines

	LES-MOST1	YSU-MOST1	MYJ-MYJ	QNSE-QNSE	ACM-MOST1	MRF-MOST1	MYNN2-MOST1
RMSE [m s^{-1}]	1.2345	1.5155	0.6317	0.4786	0.3174	0.2790	0.3275
MAE [m s^{-1}]	1.1341	1.3920	0.6088	0.3799	0.2719	0.2075	0.2279

Table 2. Performance of the simulations for the wind speed based on the comparison with the sonic anemometer measurements both in terms of the root mean square error (RMSE) and mean absolute error (MAE)

compared to the observations. This is a well-known issue in LES [13, 23]. The measurements closely follow the logarithmic profile,

$$\frac{U}{u_*} = \ln\left(\frac{z}{z_0}\right), \tag{6}$$

which is the MOST profile under neutral atmospheric conditions. It is well-known that LES under-resolves the near-surface gradients, which leads to strong wind shear within the surface layer and a mismatch for the boundary condition at the surface [24]. For YSU, the strong shear can be produced by the low jet in the wind profile. The bias between MYJ-MYJ and the observations is nearly constant with height and QNSE-QNSE follows closely MYJ-MYJ with a slight higher vertical wind shear. ACM-MOST1 is very close to the observations, MYNN2-MOST1 matches the observations extremely well, and MRF-MOST1 is the simulation closest to the logarithmic profile. The deviations between the logarithmic profile and the observations can be interpreted as the atmospheric stability conditions, in which the measurements are selected, are not truly near neutral. However, such deviations can also be attributed to the non-infinite

growing rate of turbulent eddies with height in the PBL, i.e., that the length scale of turbulence is not infinitely increasing with height as the logarithmic profile suggests [25, 26].

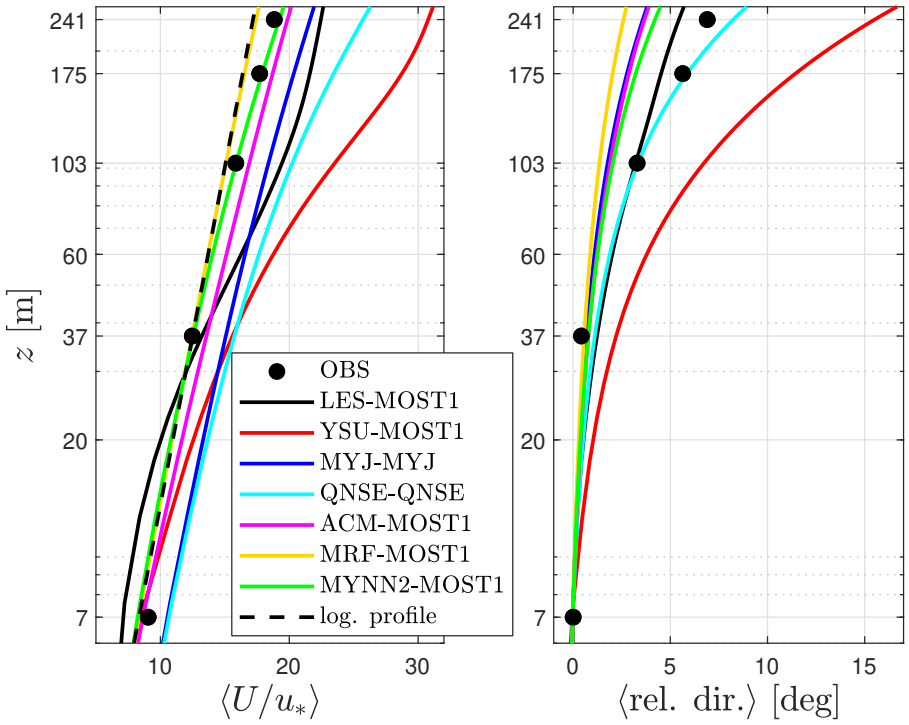

Figure 3. Spatial-average vertical profiles of normalized wind speed (left frame) and relative direction (right frame) within the range of observations of the meteorological mast at Østerild, Denmark. Observations (OBS) are represented by the black markers and simulations by the colored lines. The logarithmic (log.) profile is also shown

When looking at the relative change of wind direction within the first 250 m (Fig. 3-right frame), we found very good agreement between QNSE-QNSE, LES-MOST1, and the observations, while YSU-MOST1 clearly overestimates the observed veering, due to the low jet, MYJ-MYJ, ACM-MOST1, and MYNN2-MOST1 slightly underestimate it, and MRF-MOST1 underestimates it the most, due to the high PBL height. It is important to notice that a good match for the wind speed profile does not necessarily mean a good agreement for that of the wind direction.

Although valid for neutral atmospheric conditions only, these results are interesting for several reasons. It is seen that all simulations with PBL schemes that use MOST1, irrespective of their ability to simulate the vertical wind shear, match the MOST estimations very closely when approaching the surface. Those simulations using their own surface-layer scheme show a bias with MOST, which can be translated into a PBL driven by a lower effective roughness. This shows the importance to perform idealized simulations to evaluate PBL schemes; when evaluations are performed via, e.g., real-time simulations, 'simple' effects as those resulting from roughness assignments via land use look-up tables can be misleading. One could also think that when running real-time simulations, adjustments to the land use look-up tables should be made at the sites to compensate for any bias introduced by the surface-layer scheme.

We can also look at the vertical profile of K_m to further understand the behavior of the mean wind profile from the PBL simulations (Fig. 4-left frame). To ease the comparison and avoid problems related to the large difference between PBL heights estimated by different PBL schemes

(all PBL schemes estimate h in a different fashion), we estimate K_m from Eqn. (1) for YSU-MOST1, MRF-MOST1 and ACM2-MOST1 using the PBL height output by MYNN2-MOST1. The differences are therefore only due to differences in the simulated u_*-values; YSU-MOST1 and MRF-MOST produce the lowest and highest values, respectively. For MYNN2 and MYJ, we use Eqn. (2); for QNSE one can use the dissipation relation $\epsilon = e^3/(B_1 l)$ and $C_\mu \alpha_m = 4S_m/B_1$ with $B_1 = 16.6$ to translate K_m into the MY-form, i.e., Eqn. (2). l and q are also outputs of the QNSE scheme so the computation is straightforward. Simulations using the MYNN2 scheme also output l and q but the MYJ only outputs q, so to ease the computations we use l from MYNN2-MOST1 to compute K_m in MYJ-MYJ. Computing S_m is rather cumbersome as it depends on a number of Richardson numbers and constants that were derived by fitting the PBL scheme results to a number of LESs [8]. Thus, for simplicity, we assume the same vertical profile of S_m for the MYJ, QNSE and MYNN2 schemes, although S_m is also highly dependent on the vertical gradients of the horizontal velocity components and temperature, and we derive it following the procedure in MYNN2 [8]. The 'kinks' close to $h/z = 0.75$ appear as this is the level where l peaks the highest; above this level l in MYNN2 abruptly drops.

The result for MYNN2-MOST follows closely that of YSU-MOST1 up to $z/h \approx 0.6$, and MYJ-MYJ and QNSE-QNSE show lower values than those of MYNN2-MOST1 because of lower predicted and estimated TKE and length-scale values. Negative K_m-values can be seen for the local schemes due to the dependence on the horizontal velocity gradients close to the PBL height. In general, the vertical profiles of K_m show the expected behavior; those PBL schemes designed for simulating daytime conditions, e.g. MRF, deviate the lowest from the MOST prediction,

$$K_m = \kappa z u_*, \tag{7}$$

whereas PBL schemes designed for nighttime conditions, e.g., QNSE, deviate the largest. Such departures are also in analogy observed in the mean wind profile (Fig. 3-left frame). For completeness, we also illustrate the observed K_m values derived from the sonic-anemometer measurements using Eqn. (5). As we do know have observations of the PBL height, we also use the output of MYNN2-MOST1. As shown, the observations already deviate from MOST at the third level (103 m), and are closely followed by the MYNN2-MOST and YSU-MOST1 results.

Finally, we compare the vertical profile of the TKE computed from the sonic anemometer measurements with the simulations that provide turbulence outputs (Fig. 4-right frame). The observations show a decrease of TKE with height as expected (the result at the first measurement level is most probably due to the closeness to the ground). The results of LES-MOST1 match well the observations for the two highest levels and overestimate turbulence approaching the surface. This is most probably due to the excessive contribution of the modeled subgrid-scale TKE in the LES, which is above 20% of the total (resolved and subgrid) TKE within the first 15 levels from the ground. Increasing the horizontal resolution of LES leads to a decrease in the modeled TKE and thus to a decrease of TKE. The PBL simulations show the same behavior for the TKE profiles, MYJ-MYJ and QNSE-QNSE showing much lower values than MYNN2-MOST. The latter is found to match well the observed TKE at the highest measurement level and to follow very closely the LES-MOST1 from about 250 m up to the PBL height.

5. Conclusions and discussion

From an intercomparison of the simulations using PBL schemes and a LES within the whole PBL, we found that the MRF scheme shows the largest deviations for the potential temperature as it seemed to produce excessive vertical mixing. Thus, the vertical wind profile peaks the highest among the simulations. The YSU scheme, perhaps the most used PBL scheme in WRF, showed excessive wind shear in the lowest part of the PBL; for a mechanically induced PBL, YSU seemed to decrease boundary-layer mixing and so the jet in the wind profile was found below the temperature inversion.

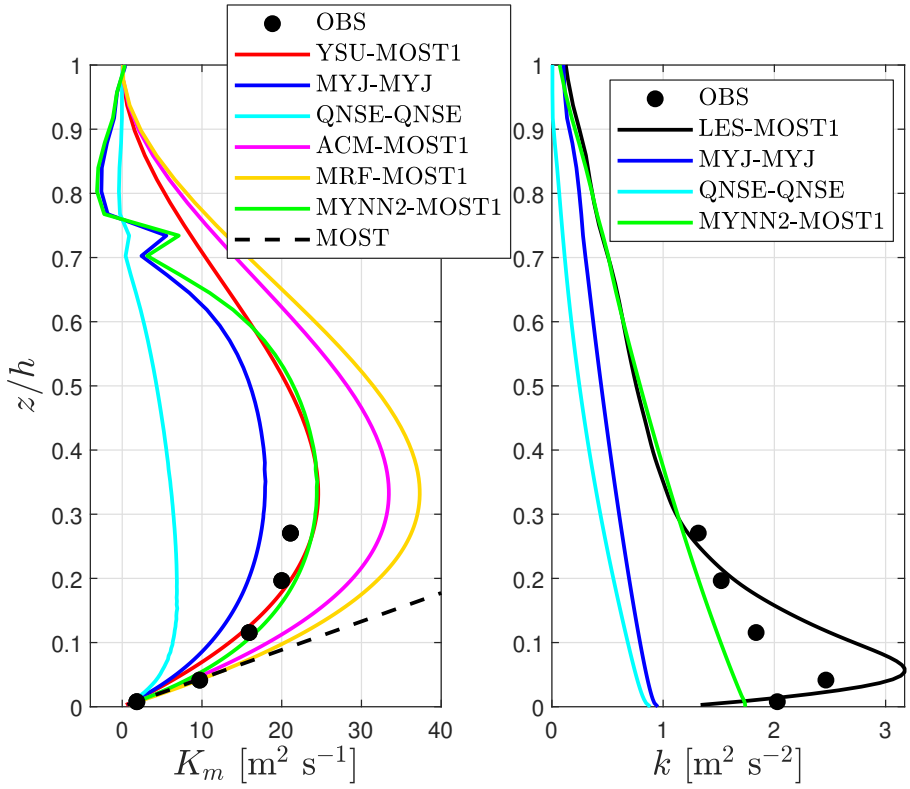

Figure 4. Spatial-average vertical profiles of momentum exchange coefficient (left frame) and turbulent kinetic energy (right frame). Observations (OBS) are represented by the black markers and simulations by the colored lines. The prediction using MOST is also shown

When comparing the simulations with the wind speed measurements, the best agreement was obtained using MYNN2-MOST1. Most importantly, we found that the simulations with PBL schemes that used their own surface-layer schemes are effectively reducing the surface roughness, as a positive bias was found for the normalized wind speed. A very good agreement between simulations and observations of the wind speed did not necessarily result in a very good agreement for the turning of the wind with height.

Intercomparison of the vertical profile of the momentum exchange coefficient between simulations using PBL schemes revealed a good match between the MYNN2 and the YSU schemes but this is due to the underestimation of the friction velocity by the latter scheme. In general, non-local PBL schemes are closer to the prediction by MOST, which does not limit the turbulence within the PBL, and local PBL schemes deviated the highest, in particular QNSE-QNSE. Sonic-anemometer derived values were closely followed by the results of the MYNN2 and YSU schemes. Further, a comparison with the sonic anemometer observations revealed that MYJ-MYJ and QNSE-QNSE strongly underestimate the TKE vertical profile and that the MYNN2-MOST profile matched well that of LES-MOST both being the closest to the observations.

Finally, we should mention that the results of evaluating idealized simulations with observations are inherently difficult to assess due to the assumptions taken both in the setup of the simulations and the methods we use to analyze the observations. One could argue that simulations using PBL schemes in this framework should be compared to LESs only. However, the latter also have known shortcomings, such as the excessive wind shear close to the ground. Simulations using PBL schemes are anyway often used ‘directly’ for wind resource assessment,

i.e., without using a microscale model to further downscale the mesoscale results. Observations are not completely stationary and we cannot guarantee that the horizontally homogeneous assumption holds above the surface layer in Østerild. Real-time simulations at the site could reveal whether or not some of these assumptions are valid, e.g., by estimating the mesoscale and turbulence tendencies for the periods of westerlies.

Acknowledgments

This work was partly funded by the Ministry of Foreign Affairs of Denmark and administered by the Danida Fellowship Centre through the "Multiscale and Model-Chain Evaluation of Wind Atlases" (MEWA) project. This work was also partly funded by the "Virtual Atmosphere" cross-cutting activity at DTU Wind Energy.

References

[1] Cohen A E, Cavallo S M, Coniglio M C and Brooks H E 2015 *Weather and Forecasting* **30** 591–612
[2] Hu X M, Nielsen-Gammon J W and Zhang F 2010 *J. Appl. Meteorol. Climatol.* **49** 1831–1844
[3] Draxl C, Hahmann A N, Peña A and Giebel G 2014 *Wind Energ.* **17** 39–55
[4] Ayotte K W, Sullivan P P, Andrén A, Doney S C, Holtslag A A M, Large W G, McWilliams J C, Moeng C H, Otte M J, Tribbia J J and Wyngaard J C 1996 *Boundary-Layer Meteorol.* **79** 131–175
[5] Dörenkämper M, Olsen B T, Witha B, Hahmann A N, Davis N N, Barcons J, Ezber Y, García-Bustamante E, González-Rouco J F, Navarro J, Sastre-Marugán M, Sile T, Trei W, Žagar M, Badger J, Gottschall J, Sanz Rodrigo J and Mann J 2020 *Geosci. Model Dev. Discuss.* 1–37
[6] Hahmann A N, Sile T, Witha B, Davis N N, Dörenkämper M, Ezber Y, García-Bustamante E, González Rouco J F, Navarro J, Olsen B T and Söderberg S 2020 *Geosci. Model Dev. Discuss.* 1–33
[7] Floors R, Hahmann A N and Peña A 2018 *J. Geophys. Res.* **123** 2718–2736 ISSN 21698996
[8] Nakanishi M and Niino H 2009 *J. Meteorol. Soc. Japan* **87** 895–912
[9] Olsen B T, Hahmann A N, Sempreviva A M, Badger J and Jørgensen H E 2017 *Wind Energ.* **2** 211–228
[10] Peña A 2019 *J. Renew. Sustain. Energ.* **11** 063302
[11] Moeng C H, Dudhia J, Klemp J and Sullivan P 2007 *Mon. Wea. Rev* **135** 2295–2311
[12] Deardorff J W 1980 *Boundary-Layer Meteorol.* **18** 495–527
[13] Mirocha J D, Churchfield M J, Muñoz Esparza D, Rai R K, Feng Y, Kosović B, Haupt S E, Brown B, Ennis B L, Draxl C, Sanz Rodrigo J, Shaw W J, Berg L K, Moriarty P J, Linn R R, Kotamarthi V R, Balakrishnan R, Cline J W, Robinson M C and Ananthan S 2018 *Wind Energ. Sci* **3** 589–613
[14] Mellor C L and Yamada T 1974 *J. Atmos. Sci.* **31** 1791–1806
[15] Hong S Y and Pan H L 1996 *Mon. Wea. Rev* **124** 2322–2339
[16] Hong S Y, Noh Y and Dudhia J 2006 *Mon. Wea. Rev.* **134** 2318–2341
[17] Pleim J E 2007 *J. Appl. Meteor. Climat.* **46** 1383–1395
[18] Janjić Z I 1990 *Mon. Wea. Rev* **118** 1429–1443
[19] Sukoriansky S, Galperin B and Peron V 2005 *Boundary-Layer Meteorol.* **117** 231–257
[20] Monin A S and Obukhov A M 1954 *Trudy Geofiz. Inst. AN SSSR* **24** 163–187
[21] Högström U 1988 *Boundary-Layer Meteorol.* **42** 55–78
[22] Mass C F, Ovens D, Westrick K and Colle B A 2002 *Bull. Amer. Meteor. Soc.* **83** 407–430
[23] Kosović B 1997 *J. Fluid Mech.* **336** 151–182
[24] Maronga B, Knigge C and Raasch S 2020 *Boundary-Layer Meteorol.* **174** 297–325
[25] Gryning S E, Batchvarova E, Brümmer B, Jørgensen H and Larsen S 2007 *Boundary-Layer Meteorol.* **124** 251–268
[26] Peña A, Gryning S E and Mann J 2010 *Q. J. Royal Meteorol. Soc.* **136** 2119–2131